Cross-sectional scanning tunneling microscopy of epitaxial GaAs structures

A. Vaterlaus,[a] R. M. Feenstra, P. D. Kirchner, J. M. Woodall, and G. D. Pettit

IBM Research Division, T. J. Watson Research Center, Yorktown Heights, New York, 10598

The scanning tunneling microscope is used to study GaAs epitaxial structures, cleaved in ultrahigh vacuum, and viewed in cross section. Two applications are described: in the first, the net donor concentration in Si-doped GaAs is deduced by direct measurement of the depletion width at *pn* junctions. In the vicinity of the *pn* junctions, net donor concentrations of greater than 2×10^{19} cm^{-3} are observed. This interfacial donor activity is an order-of-magnitude higher than that found in the bulk. In the second application, low-temperature-grown and annealed GaAs is studied. Arsenic precipitates are observed in the material. The precipitates are found to produce electronic states within the GaAs band gap, and these states cause the Fermi level to be pinned near midgap.

I. INTRODUCTION

For the past decade, the scanning tunneling microscope (STM) has been used to study the geometric and electronic structure of surfaces. Since the tunnel current is dominated by contributions from the outermost layer of atoms, the information obtained generally reflects the properties of the surface itself. In this work, we describe "cross-sectional" studies with the STM intended to probe features which are *not* determined specifically by the surface, but rather, are indicative of the underlying bulk material. The materials studied here are GaAs layered structures grown by molecular-beam epitaxy (MBE). The cross-sectional studies consist of cleaving the wafer in ultrahigh vacuum, positioning the STM probe tip over the layers of interest, and performing imaging and spectroscopic measurements. GaAs is a convenient material to use for these studies, since the (110) cleavage plane is naturally passivated in the sense that the energies of the surface dangling bonds lie outside of the band gap. Thus, spectroscopic measurements do indeed reflect properties of the material beneath the surface. Cross-sectional STM studies have previously been performed on GaAs/AlGaAs interfaces by Salemink and co-workers.[1] For the case of silicon, the occurrence of dangling bond states within the band gap requires some type of surface passivation to enable cross-sectional studies. This has recently been accomplished using *ex situ* hydrogen termination by Johnson *et al.*[2]

In this work, we describe two applications of the STM cross-sectional technique. First, we discuss results obtained on GaAs *pn*-doping superlattices, consisting of alternating layers of *n*- and *p*-type material. In previous studies, we found that the *n*- and *p*-type layers can be clearly distinguished in STM images and spectroscopic measurements.[3,4] Also, the depletion regions which occur at *pn* junctions can be directly observed. By measuring the width of the depletion regions, we can deduce the doping concentration of the semiconductor. We use this method here to study Si doping of GaAs. Silicon is an amphoteric dopant in GaAs, forming a donor when substituting for Ga and an acceptor when substituting for As. At low concentrations, Si energetically prefers to form donors, but at high concentrations thermodynamic equilibrium tends to drive Si into acceptor sites.[5] The net donor concentration (difference between total donor and acceptor concentrations) is thus limited to about 3×10^{18} cm^{-3} in bulk GaAs. It is of interest to obtain higher donor concentrations for particular device structures, e.g., δ-doped layers, and it has been found in certain cases that higher concentrations can be obtained, at least in a narrow regions near the wafer surface or near a *pn* junction.[5] However, in such cases it is difficult to measure directly what the net donor concentration actually is. Here, we use the STM to directly measure donor concentrations as a function of Si-doping concentration. In the vicinity of the *pn* junctions, we observe net donor concentrations of greater than 2×10^{19} cm^{-3}. This interfacial donor activity is an order-of-magnitude higher than that found in the bulk.

The second work described here is the study of GaAs grown at low temperatures, near 200 °C, and subsequently annealed at 600 °C. The low-temperature-grown material is known to be nonstoichiometric, containing 1%–2% excess arsenic.[6] In unannealed material, the excess arsenic is believed to form point defects, e.g., an antisite defect consisting of As on a Ga site. In annealed material, the excess arsenic agglomerates to form precipitates.[7] The resulting material is found to be semi-insulating, and thus has useful device applications.[8] In this study, we use the STM to directly observe the arsenic precipitates and to measure their electrical properties. We find that the low-temperature-grown and annealed (LTA) layers have their Fermi level pinned near midgap. The states responsible for the pinning arise from the arsenic precipitates, and are seen in spectroscopy as tails of states extending out of the valence and conduction bands.

In general, the results of spectroscopic STM measurements on GaAs(110) depend on the degree of surface Fermi-level pinning due to steps or residual contamination of the surface. This point is discussed in detail in Ref. 4 for

[a] Permanent address: FKP-Mikrostrukturforschung, ETH Hoenggerberg, HPT C2.2, 8093 Zurich, Switzerland.

the case of cross-sectional studies; surface pinning is found to affect the spectra in two ways. First, dopant-induced components in the tunnel current (arising from electrons tunneling out of filled conduction band states on n-type material or into empty valence band states on p-type material) which are seen on flat, unpinned surfaces are absent on rough, pinned surfaces.[9,10] Second, tip-induced band bending which modifies the spectra for low-doped material (e.g., in the depletion region of a pn junction[3]) is decreased for pinned surfaces because of the presence of surface charge. In this work, the results of Sec. III were obtained from relatively rough cleaves, in which some surface pinning occurs. The results of Sec. IV were obtained from flat, ideal cleaves in which the effects of surface pinning are negligible, as evidenced by the spectra displayed there.

II. EXPERIMENT

The structures discussed here were grown by molecular-beam epitaxy in a Varian GEN II system. The doping superlattice described in Sec. III consists of alternating layers of n- and p-type material, grown at 550 °C. The p dopant is C, at a concentration of 3×10^{19} cm^{-3}. The n dopant is Si, with concentration varying from 10^{17} to 10^{20} cm^{-3} in successive layers. The LTA GaAs discussed in Sec. IV was grown at 200 °C, and subsequently annealed at 600 °C for 30 min under an As pressure of 10^{-6} Torr. The LTA layers are n-type, doped with Si at a concentration of 1×10^{19} cm^{-3}, and have thickness of 500 Å. These layers are surrounded on both sides by 500 Å thick p-type layers (Be-doped at 5×10^{19} cm^{-3}) grown at 350 °C, which serve as markers for the LTA layer, and n-type layers (Si-doped at 1×10^{19} cm^{-3}) grown at 350–600 °C surround the p-type layers. Samples measuring $0.6 \times 0.1 \times 0.015$ in. were cut from the wafers. AuGe ohmic contacts were applied to both sides of the samples. Cleavage was accomplished by notching the sample on one edge at the midpoint of the long side, mounting it with half of the long side extending out of the holder, and then pressing on the face of this protruding piece to cleave it at the notch. The quality of the cleaves varied; in some cases nearly perfect cleavage faces were obtained, but generally some steps occurred on the cleavage face especially on its front edge near the grown structure.

The STM used for these studies has been previously described, including the stepping motion used for locating the superlattice.[11] STM images were obtained with a constant tunnel current of typically 0.1 nA, and at various voltages specified below. Spectroscopic measurements were performed using a method previously developed which obtained a large dynamic range in the tunnel current and conductivity.[12] Briefly, the tip-sample separation is varied as the voltage is scanned according to $\Delta s = -a|V|$, with $a \simeq 1$ Å/V. Subsequent normalization to constant s is accomplished by multiplying the measured current or conductivity by $\exp(2\kappa \Delta s)$, where the decay constant κ is measured during each experiment and has values in the range 0.7–1.1 Å^{-1}. Conductivity was measured using a lock-in amplifier, with typically 50 mV modulation on the bias
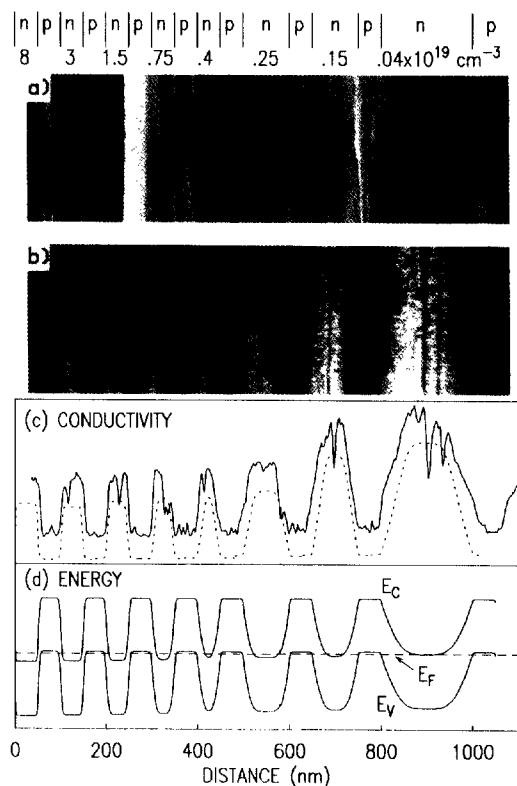
FIG. 1. The GaAs doping superlattice is shown at the top of the figure, with n-type (Si) doping concentrations listed, and a p-type (C) concentration of 3×10^{19} cm^{-3}. Constant-current STM topograph and the conductivity image are shown in (a) and (b) respectively, acquired with sample voltage of -2.0 V. Panel (c) shows a line profile of the measured conductivity (solid line), and model calculation (dotted line). A band diagram is shown in (d), computed assuming 100% donor incorporation of Si.

voltage. Conductivity images were thus acquired simultaneously with the usual constant-current topography.

III. SILICON DOPING OF GaAs

Figure 1 shows the doping superlattice used for this study. The structure consists of alternating layers of n- and p-type material, with graded n-type (Si) concentration and varying width of the layers to allow measurement of an entire depletion width at each pn junction. Figure 1(a) shows a constant-current STM topograph obtained from this superlattice, and Fig. 1(b) shows an associated conductivity image measured at constant current. The topograph displays a number of surface steps (single, double, triple, and larger steps are present), which obscure the direct observation of the superlattice. However, the superlattice is directly seen in the conductivity image, with the brighter regions corresponding to n-type material and the darker regions p-type material. Some of the large steps in the topograph produce individual thin lines in the conductivity (due to the presence of surface states). At the pn junctions, the measured conductivity varies monotonically from its value in the n-type material to its value in the p-type material.

STM conductivity images can be directly interpreted in terms of the position of the valence band (VB) or conduc-
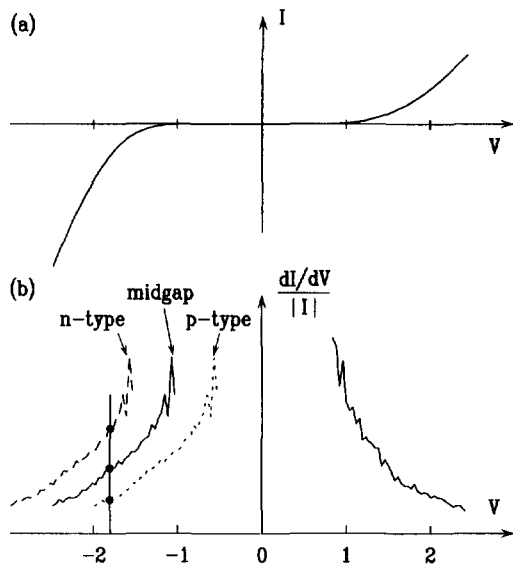
(a)

(b)

FIG. 2. Schematic illustration of the interpretation of STM conductivity images. A typical curve of tunnel current vs sample voltage is shown in (a), and (b) shows the ratio of conductivity to current (solid lines). At a given negative voltage, this ratio is larger on n-type material in which the I-V curve shifts to the left (dashed line), and smaller on p-type material in which the I-V curve shifts to the right (dotted line).

tion band (CB) edges relative to the Fermi level, as illustrated in Fig. 2. In Fig. 2(a) we plot a typical current–voltage (I-V) curve from a GaAs(110) surface, acquired in this case with fixed tip-sample separation and from a surface region in which the Fermi level (0 V) is pinned near midgap. A region of low current, extending from about -1 to $+1$ V can be seen, corresponding approximately to the location of the GaAs band gap (when the current in viewed on a logarithmic scale, the band edges are seen more accurately to be located at about -0.7 and $+0.7$ V, giving the correct band gap of 1.4 eV). In conductivity images, one measures the conductivity at constant current, which is proportional to the ratio of conductivity to current, $(dI/dV)/I$. We plot this quantity in Fig. 2(b). A conductivity image corresponds to measuring $(dI/dV)/I$ at a given voltage, and scanning over surface regions in which the position of the band edges may vary due to a change in the doping. As shown in Fig. 2(b), on n-type material the I-V curve shifts to the left, thus increasing the measured conductivity, and on p-type material the I-V curve shifts to the right, thus decreasing the conductivity. Thus, at negative voltage, n-type material appears bright in the conductivity image and p-type material appears dark, as seen in Fig. 1(b). The opposite conclusion holds for positive sample voltage.

The variation in measured conductivity across the superlattice can be more clearly seen in the profile shown by the solid line in Fig. 1(c), obtained by summing the individual scans of the image in Fig. 1(b). It is evident that the transition from n- to p-type behavior becomes sharper as the Si concentration increases, reflecting a decrease in the depletion width. Qualitatively, this behavior agrees with that which is seen in a band diagram for the superlattice, as

shown in Fig. 1(d), which is computed assuming 100% Si incorporation as a donor. For example, for the lowest doped n-type layer one expects a depletion width of $w = (2\epsilon E_g/e^2 N_D)^{1/2} = 71$ nm, for dielectric constant of $\epsilon = 12.9\epsilon_0$, band gap of $E_g = 1.43$ eV, and $N_D = [\mathrm{Si}] = 4 \times 10^{17}$ cm^{-3}. Both the conductivity profile and the band diagram in Figs. 1(c) and (d) show this broad depletion region at the junction of this n-type layer. Alternatively, for the highly doped layer with $[\mathrm{Si}] = 8 \times 10^{19}$ cm^{-3}, the depletion width is only about 10 nm (limited in part by the 3×10^{19} cm^{-3} doping of the p-type layer), and a correspondingly narrow transition is seen at the pn junctions of this layer.

To quantify the relationship between the observed conductivity and the depletion widths, we must adopt some model to describe the conductivity. The simplest approximation is to assume a linear onset for the tunneling current at the conduction or valence band edge,

$$\frac{dI}{dV} = \frac{I_0}{(V - V_0)} , \tag{1}$$

where I_0 is the constant current maintained during the conductivity measurement, V is the sample voltage, and V_0 is the position of the band edge. This equation illustrates the dominant behavior of the conductivity, namely, it diverges as the voltage approaches the band edge. A more realistic form for the conductivity can be obtained by generalizing Eq. (1) in the following manner:

$$\frac{dI}{dV} = \frac{\alpha I_0}{(V - \alpha V_0)^\beta} . \tag{2}$$

The parameters a and β account for oversimplifications in the form of Eq. (1): voltage dependence of the tunneling transmission produces $a \gg 1$ with $a \to 1$ as $V \to V_0$, and the decrease in state concentration to zero at the semiconductor band edge produces $\beta < 1$, with $\beta \to 0$ as $V \to V_0$ (Refs. 12, 13). With these parameters, Eq. (2) provides a good description of the conductivity versus voltage measurements shown in Fig. 2. Effects of surface pinning will cause the surface Fermi-level position to deviate from that in the bulk, so that we must take V_0 to be the band edge position relative to the *surface* Fermi level. This can be written as

$$eV_0 = x(E_b - E_F) + (1 - x)(E_b - E_p), \tag{3}$$

where E_b is the band edge ($b = V$ or C), E_p in the midgap pinning position (the charge-neutrality level[14]), and the parameter x describes the strength of the pinning, with $x = 1$ corresponding to an unpinned surface. Finally, the parameter α in Eq. (2) describes the role of tip-induced band bending on the conductivity characteristic. We expect this effect to be relatively small in the present case because of the surface pinning.[4] Band bending will tend to stretch out the conductivity characteristic, corresponding to $\alpha > 1$.

In Fig. 3(a) we present several computations of the conductivity profile across an n-type layer. We use as an example the band diagram from the lowest doped layer in Fig. 1. For reference, the inverted band diagram is shown by the solid line in Fig. 3(a). We then compute conductivity from Eq. (2) for two choices of the parameters: (1)
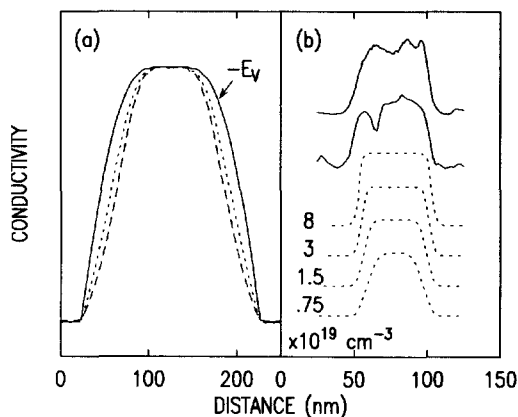
FIG. 3. (a) Model computations of conductivity profiles, using parameter sets (1) dashed line, and (2) dotted line, as described in text. For comparison, an inverted band profile is shown by the solid line. (b) Experimental results (solid lines) for $[Si]=3\times10^{19}$ cm^{-3} layer, compared with model calculations (dotted lines) for the donor concentrations listed.
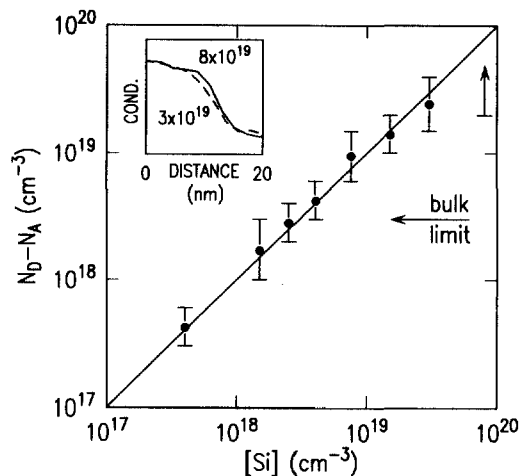

FIG. 4. Net donor concentration vs silicon concentration, obtained from an analysis of the observed depletion widths in the GaAs doping superlattice. A typical bulk limit for the Si donor concentration of 3×10^{18} cm^{-3} is indicated. The inset shows the conductivity transition from p-type (right side) to n-type (left side) for $[Si]=3\times10^{19}$ cm^{-3} (dashed line) and 8×10^{19} cm^{-3} (solid line).

the simplest case with $x=\alpha=a=\beta=1$, and (2) a more realistic case, with $x=0.5$, $\alpha=1.5$, $\beta=0.5$, and $a=2$. The model computations shown in Fig. 3(a) have been adjusted so that their minimum and maximum values equal those values for the inverted band diagram. It is clear from these results that the width of the conductivity characteristic is not sensitive to the parameters used in Eq. (2). Thus, we are justified in using Eq. (2) to fit the observed conductivity data. To be specific, we will use the parameter set given by choice (2) above.

A comparison of the observed conductivity profile to the model calculation is shown in Fig. 1(c). The calculations use the band diagram of Fig. 1(d), which is computed assuming 100% incorporation of Si as a donor. The model result for each n-type layer is adjusted in terms of minimum and maximum value to match the data. The width of the theoretical curves then gives a direct indication of the net donor concentration in the GaAs. We find good agreement between the model calculation and the observed conductivity. A more detailed comparison is made in Fig. 3(b), where we show two experimental results for the conductivity across the 3×10^{19} cm^{-3} layer, and model results for donor concentrations of 8, 3, 1.5, and 0.75×10^{19} cm^{-3}. The results can be compared on the basis of both the overall width of the profile and the sharpness of the transition from low to high conductivity. We see that the experimental results in Fig. 3(b) match best with the middle two model calculations, and the net donor concentration is thus estimated to be in the range $(1.5–4)\times10^{19}$ cm^{-3}. A similar comparison between experiment and theory is made for each of the n-type layers.

Our results for the determination of the net donor concentration in the GaAs n-type layers are summarized in Fig. 4. We find that, within the overall uncertainty of a factor of 2–3, all of the silicon is incorporated as donors in the GaAs. For the most highly doped layer with $[Si]=8\times10^{19}$ cm^{-3} we can only determine a lower bound on the donor activity since the depletion width is limited by the p-layer doping. However, as shown in the inset of Fig.

4, we do observe a smaller depletion width for the 8×10^{19} cm^{-3} layer compared with the 3×10^{19} cm^{-3} layer, thus demonstrating that the net donor concentration increases monotonically all the way up to $[Si]=8\times10^{19}$ cm^{-3}.

IV. LOW-TEMPERATURE-GROWN AND ANNEALED GaAs

In this section, we describe our cross-sectional STM results obtained from GaAs which has been low-temperature grown, and subsequently annealed (LTA). An STM image of the material is shown in Fig. 5, showing both topography and conductivity. As marked in the conductivity image, the LTA layer occurs at the left-hand side
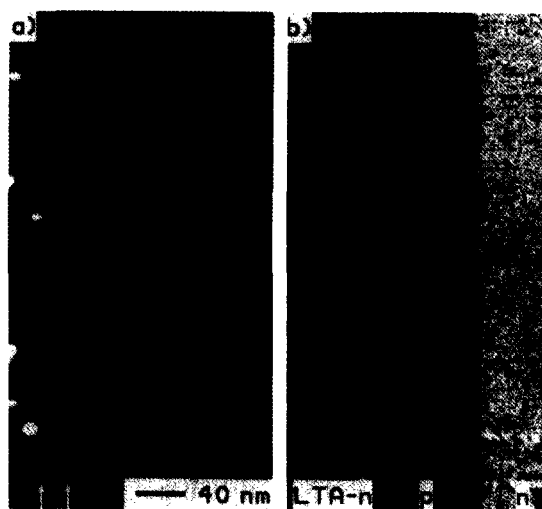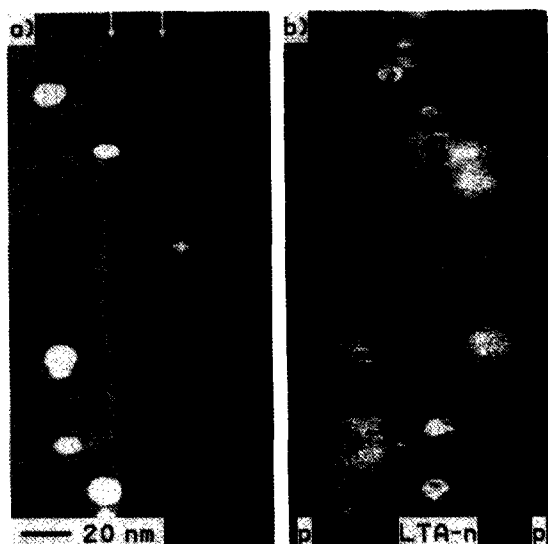

FIG. 5. STM image of a cleaved GaAs structure, showing (a) topography and (b) conductivity, acquired at a sample voltage of -2.5 V. As indicated in (b), the structure contains an LTA n-type layer, bordered by p- and n-type layers grown at higher temperature. Two steps occur in the LTA layer, as marked by arrows in (a).

FIG. 6. STM image of a cleaved GaAs structure, showing (a) topography and (b) conductivity, acquired at a sample voltage of −2.5 V. As indicated in (b), the structure contains an LTA n-type layer, surrounded by p-type layers grown at higher temperature. Two steps occur in the LTA layer, as marked by arrows in (a).
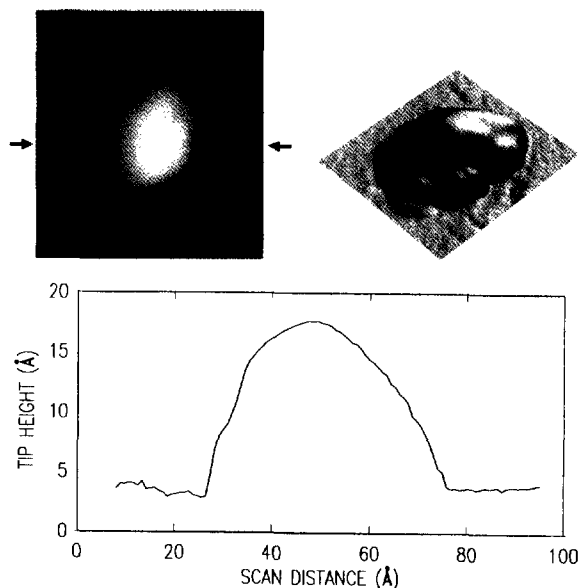

FIG. 7. STM image of an individual arsenic precipitate. A topograph is shown in the upper left, with the grey scale corresponding the surface height. The same precipitate is shown in a perspective view in the upper right, with the shading determined by a surface derivative. A line cut through the precipitate, taken along the position indicated by arrows in the topograph, is shown in the lower part of the figure.

of the image, the neighboring p layer is in the center of the image, and an n-type buffer layer occurs at the right-hand side of the image. An expanded view of the LTA layer is shown in Fig. 6. Small protrusions can be seen in the LTA layer, appearing as white circular areas in Figs. 5(a) and 6(a), with a typical diameter of 50 Å and height of 15 Å. Such protrusions are never seen on n- or p-type material grown at temperatures of 350 °C or higher, and thus we identify the protrusions with the arsenic precipitates which are known to occur in this material.[3] Based on the observed number of protrusions, we estimate a precipitate density of 6×10^{16} cm^{-3}, in reasonable agreement with that found in transmission-electron microscopy (TEM) studies.[15] In addition to the precipitates present in Fig. 6(a), several depressions or "holes" are visible in the image, appearing as the dark circular areas with a typical diameter of 50 Å. We associate these holes with regions where an arsenic precipitate has been pulled out of the material during the cleave (in general, one expects the same number of protrusions as depressions in the images). An expanded view of one precipitate is shown in Fig. 7. The outer surface of the precipitates generally appears rather rough and bumpy, although individual atomic features have not been resolved.

The conductivity images shown in Figs. 5(b) and 6(b) provide some information on the electrical properties of the LTA layers. As discussed in the previous section, these conductivity images can be directly interpreted simply by noting that the conductivity at constant current increases monotonically as the voltage approaches the band edge. Thus, the n-type buffer layer in Fig. 5(b) has the highest conductivity (lowest energy VB edge), the LTA n layer has an intermediate conductivity, and the p-type layer has the lowest conductivity (highest energy VB edge). From

Fig. 6(b), it is apparent that the precipitates generally appear darker in conductivity than the surrounding GaAs regions of the LTA layer. The origin of these electrical properties can be understood from complete spectral measurements acquired from the various locations, as discussed below.

In Fig. 8 we show conductivity versus voltage measurements acquired from the LTA GaAs. In all cases the spectra are acquired from regions of the sample far removed from any surface steps, so that effects of surface Fermi-level pinning are absent in the data. Figures 8(a) and (b) show results acquired from the p-type and n-type layers grown at "normal" temperatures (above 350 °C). These spectra show highly ideal behavior, with well-defined conduction and valence band edges. Also, "dopant-induced" (D) components of the tunnel current are seen in the spectra. As shown in the insets of Figs. 8(a) and (b), these components arise from tunneling out of the filled conduction band state or into empty valence band states for n- and p-type material, respectively. The existence of these components provides strong evidence of the ideal, unpinned nature of the surface.[9,10]

Figures 8(c) and (d) shows spectroscopy results obtained from the LTA layer. Spectra were acquired on the precipitates themselves, and on regions of the bare GaAs in between the precipitates. The results shown are the average of about ten such spectra at each type of location. On the bare GaAs, we see a band gap extending from about −0.65 to +0.8 eV, indicating a pinned Fermi level at $E_F = E_V + 0.65$ eV. No states are visible in the gap for the GaAs spectra. On the precipitates, we observe a band gap at about the same location, but now tails of states are observed extending into the gap. These gap states are most
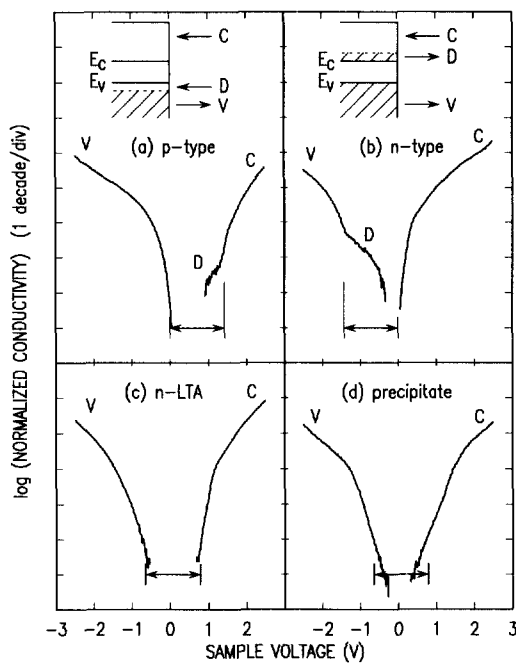
FIG. 8. STM spectrum acquired from various spatial location on the LTA GaAs material: (a) and (b) on *p*- and *n*-type layers grown at "normal" temperatures of above 350 °C, (c) on the *n*-type layer grown at a low temperature of 200 °C and annealed (LTA), and (d) on an arsenic precipitate in the LTA layer. Diagrams of the components of the tunnel current are shown in the upper part of the figure for flatband *n*- and *p*-type material, with the components denoted by *C*—conduction band, *V*—valence band, and *D*—dopant induced. The dotted lines in the diagrams denote the Fermi-level position (shown inside the bands, for the case of high doping). The arrows in the lower part of each panel show the estimated position of the band gap relative to the observed spectrum. The sample voltage corresponds to the energy of a state relative to the Fermi level (0 V).

states anywhere within the LTA layer, we identify the precipitates as being responsible for the Fermi-level pinning observed throughout the LTA layer.

V. CONCLUSIONS

In this work, we describe two applications of the STM cross-sectional method. In the first, we demonstrate how the STM can be used to measure the net donor concentration of Si-doped GaAs. In the vicinity of *pn* junctions, we observe net donor concentrations of greater than 2×10^{19} cm^{-3}. This is the highest donor activity ever reported in GaAs (approaching the solubility limit), and exceeds typical limits on bulk electron concentration by an order of magnitude. The mechanism for this large interfacial donor activity is believed to be the stabilization of the Fermi level near the bottom of the band gap (due to the nearby *p* layers), which prevents the formation of Si acceptors in the GaAs.[5]

In the second application of cross-sectional STM, we study LTA GaAs grown at 200 °C and subsequently annealed at 600 °C. We observe arsenic precipitates in the material. The size and number density of the precipitates is found to be in good agreement with that measured by TEM.[15] The Fermi level in the LTA *n*-type material is observed to be pinned near midgap. Electronic states extending into the band gap are observed at the precipitates, and these states are identified as being responsible for the Fermi-level pinning in the material.

ACKNOWLEDGMENT

pronounced on the conduction band side of the spectrum, but can also be seen on the valence band side. These midgap states are shown in more detail in Fig. 9, where we plot the data in normalized form as the ratio of differential to total conductivity.[12] Since these gap states are only observed on the precipitates, and are the only source of gap

[1]H. W. M. Salemink, O. Albrektsen, and P. Koenraad, Phys. Rev. B **45**, 6946 (1992); H. W. M. Salemink and O. Albrektsen, J. Vac. Sci Technol. B **10**, 1799 (1992).

[2]M. B. Johnson and J.-M. Halbout, J. Vac. Sci. Technol. B **10**, 508 (1992); E. T. Yu, M. B. Johnson, and J.-M. Halbout, Appl. Phys. Lett. **61**, 201 (1992).

[3]R. M. Feenstra, E. T. Yu, J. M. Woodall, P. D. Kirchner, C. L. Lin, and G. D. Pettit, Appl. Phys. Lett. **61**, 795 (1992).

[4]R. M. Feenstra, A. Vaterlaus, E. T. Yu, P. D. Kirchner, C. L. Lin, J. M. Woodall, and G. D. Pettit, *Semiconductor Interfaces at the Subnanometer Scale*, NATO ASI Series E No. 243, edited by H. W. M. Salemink and M. D. Pashley (Kluwer, Dordrecht, 1993), p. 127.

[5]P. D. Kirchner, T. N. Jackson, G. D. Pettit, and J. M. Woodall, Appl. Phys. Lett. **47**, 26 (1985).

[6]M. Kaminska, Z. Liliental-Weber, E. R. Weber, T. George, J. B. Kortright, F. W. Smith, B.-Y. Tsaur, and A. R. Calawa, Appl. Phys. Lett. **54**, 1881 (1989).

[7]M. R. Melloch, N. Otsuka, J. M. Woodall, A. C. Warren, and J. L. Freeouf, Appl. Phys. Lett. **57**, 1531 (1990).

[8]F. W. Smith, A. R. Calawa, Chang-Lee Chen, M. J. Mantra, and L. J. Mahoney, IEEE Electron Device Lett. **EDL-9**, 77 (1988).

[9]R. M. Feenstra and J. A. Stroscio, J. Vac. Sci. Technol. B **5**, 923 (1987).

[10]J. A. Stroscio and R. M. Feenstra, J. Vac. Sci. Technol. B **6**, 1472 (1988).

[11]R. M. Feenstra, *Proceedings of the 21th International Conference on the Physics of Semiconductors*, edited by P. Jiang and H.-Z. Zheng (World Scientific, Singapore, to be published).

[12]P. Mårtensson and R. M. Feenstra, Phys. Rev. B **39**, 7744 (1988).
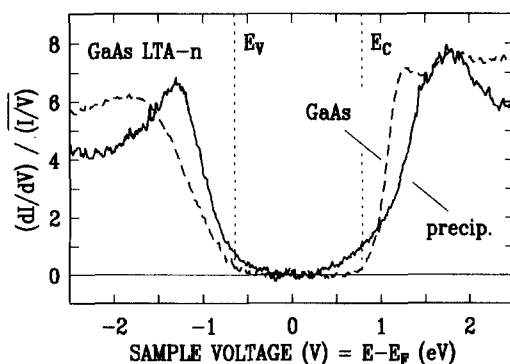

FIG. 9. STM spectra acquired from the LTA *n*-type layer. Spectra are shown acquired on the arsenic precipitates (solid line) and on regions of bare GaAs in between the precipitates (dashed line). The valence and conduction band edges are marked by E_V and E_C, respectively.

[13]R. M. Feenstra, J. A. Stroscio, and A. P. Fein, Surf. Sci **181**, 295 (1987).

[14]F. Flores, J. C. Durán, and A. Muñoz, Phys. Scr. T **19**, 102 (1987).

[15]A. C. Warren, J. M. Woodall, P. D. Kirchner, X. Yin, F. Pollack, M. R. Melloch, N. Otsuka, and K. Mahalingam, Phys. Rev. B **46**, 4617 (1992). The density of protrusions seen in STM should correspond to only about half the precipitate density observed in TEM, since the other half of the precipitates appear as holes in the STM images.